THE ROYAL SOCIETY

*Received* 16 December 2003
*Accepted* 22 March 2004
*Published online* 9 June 2004

# Cranial mechanics and feeding in *Tyrannosaurus rex*

**Emily J. Rayfield**

*Department of Earth Sciences, University of Cambridge, Downing Street, Cambridge CB2 3EQ, UK* (*eray@esc.cam.ac.uk*)

It has been suggested that the large theropod dinosaur *Tyrannosaurus rex* was capable of producing extremely powerful bite forces and resisting multi-directional loading generated during feeding. Contrary to this suggestion is the observation that the cranium is composed of often loosely articulated facial bones, although these bones may have performed a shock-absorption role. The structural analysis technique finite element analysis (FEA) is employed here to investigate the functional morphology and cranial mechanics of the *T. rex* skull. In particular, I test whether the skull is optimized for the resistance of large bi-directional feeding loads, whether mobile joints are adapted for the localized resistance of feeding-induced stress and strain, and whether mobile joints act to weaken or strengthen the skull overall. The results demonstrate that the cranium is equally adapted to resist biting or tearing forces and therefore the 'puncture–pull' feeding hypothesis is well supported. Finite-element-generated stress–strain patterns are consistent with *T. rex* cranial morphology: the maxilla–jugal suture provides a tensile shock-absorbing function that reduces localized tension yet 'weakens' the skull overall. Furthermore, peak compressive and shear stresses localize in the nasals rather than the fronto-parietal region as seen in *Allosaurus*, offering a reason why robusticity is commonplace in tyrannosaurid nasals.

**Keywords:** finite element method; *Tyrannosaurus*; Dinosauria; Theropoda; feeding; kinesis

## 1. INTRODUCTION

Evidence from tooth-marked bones, tooth morphology and coprolites suggests that the large theropod dinosaur *Tyrannosaurus rex* fed using a 'puncture–pull' feeding strategy (*sensu* Erickson & Olson 1996), in which an extremely powerful, potentially bone-crushing bite was followed by drawing teeth through flesh and bone. *Tyrannosaurus rex* cranial bones are expanded, robust elements in contrast to most other theropod crania (figure 1*a*), while the teeth are notable for their stout, almost peg-like, morphology (Farlow *et al.* 1991; Abler 1992, 1999), consistent with ideas of powerful bite force production (Molnar & Farlow 1990; Erickson *et al.* 1996; Chin *et al.* 1998; Meers 2002). If the puncture–pull strategy was to be effective, the skull must have been capable of withstanding not only high magnitude loading during biting but also resisting indirect loads at the teeth generated by neck and body musculature during the 'pull' phase of feeding.

Despite an overall increase in cranial robustness, individual skull bones are often loosely articulated together and dermal sutures in the lateral sidewalls of the skull are frequently patent (unfused) (figure 1*a*). This open framework arrangement has been hypothesized as providing a shock-absorption mechanism (Buckley 2003), with notable cranial movement (Larson 1998) or streptostyly without significant kinesis (Molnar 1991). The idea that patent sutures are adapted to provide localized stress and strain resistance remains to be tested, as does the overall effect of patent sutures on cranial strength and capacity.

There can be no doubt that these loose articulations affected the mechanical performance of the *T. rex* skull during biting. Experimental work on living animals has revealed that strains induced by biting or muscular loading are absorbed and therefore differentially transmitted across sutures in the skulls of lizards, miniature pigs, goats and sheep (Smith & Hylander 1985; Jaslow 1990; Jaslow & Biewener 1995; Rafferty & Herring 1999; Herring 2000; Herring & Teng 2000; Thomason *et al.* 2001; Rafferty *et al.* 2003). It has also been shown that during dynamic impact loading, interdigitating sutures absorb strain energy and dampen impact forces more effectively than cranial bone, facilitating load dissipation and protecting cranial bones from fracture (Jaslow 1990). Nevertheless, associated sutural soft tissues may be highly strained (Smith & Hylander 1985; Jaslow & Biewener 1995) and despite their protective role, sutures may represent zones of deformation and weakness within the skull (Herring 2000). In light of this evidence, it is therefore surprising that in the crania of large forcefully biting animals such as *T. rex*, patent sutures persist between most facial bones.

This analysis investigates whether the cranium of *T. rex* was 'designed' in a way to mechanically resist loading conditions induced by a puncture–pull feeding regime. Implicit to this analysis is the role sutures play in modifying the stress environment of the cranium during function. Do sutures act in an adaptive fashion to dissipate strain and protect bony tissues, perhaps making the skull 'stronger,' or is a flexible patent skull a 'design flaw' in terms of resisting feeding forces, leading to an overall 'weaker' structure?

Visualizing skeletal stress and strain during function provides an insight into skeletal design and optimization, and the finite element method (FEM) is one technique that offers such an opportunity (Thomason 1995). The FEM permits an assessment of the mechanical behaviour of digitally manipulated structures as varied as bridges, racing cars and human femora. FE analysis (FEA) has recently been co-opted to palaeontology to investigate the mechanical behaviour of fossil skeletal material (Jenkins 1997; Rayfield 1998; Rayfield *et al.* 2001; Fastnacht *et al.*


© 2004 The Royal Society

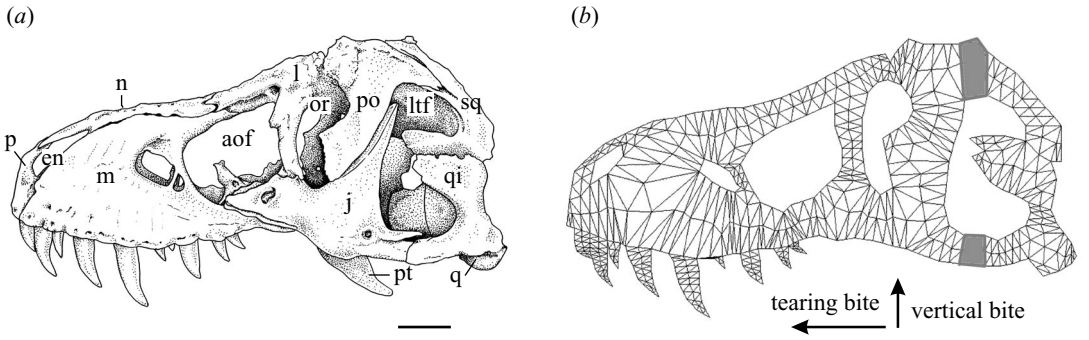


Figure 1. *Tyrannosaurus rex* skull and FEM. (*a*) Skull of BHM 3033, left lateral view; and (*b*) 2D FE-mesh of BHM 3033 depicting skull as 'fused' without mobile sutures. Grey areas indicate surfaces constrained from moving in all translatory directions, arrows indicate direction of bite force applied to all teeth, either vertical or horizontal 'tearing'. Abbreviations: aof, antorbital fenestra; en, external naris; j, jugal; l, lacrimal; ltf, lower temporal fenestra; m, maxilla, n, nasals; or, orbit; p, premaxilla; po, postorbital; pt, pterygoid; q, quadrate; qj, quadratojugal; sq, squamosal. Scale bar 10 cm.

2002; Jenkins *et al.* 2002; Snively & Russell 2002), including large theropod crania (Rayfield *et al.* 2001, 2002).

All previous FEMs have treated the skull as a single unit (e.g. Rayfield *et al.* 2001). In this paper, the stress environment of a fused FE-skull model is assessed, after which results obtained from the fused skull model are used to predict the mechanical effect of introducing regions of mobility. Introducing simple sutural contacts into the FEM then permits an evaluation of these predictions. Such investigation highlights the potential of FEA in testing hypotheses of cranial design and evolution. The results of the FEM system have implications for the suitability of puncture–pull as a feeding strategy for *T. rex* and the functional significance, if any, of maintaining patent sutures between cranial bones in an animal with an apparently bone-crushing bite.

## 2. MATERIAL AND METHODS

Specimens studied: AMNH 5027: American Museum of Natural History, New York; BHM 3033: Black Hills Museum, Hill City, South Dakota; MOR 555: Museum of the Rockies, Bozeman, Montana; SDSM 12047: South Dakota School of Mines, Rapid City, South Dakota; RTMP 81.6.1: Royal Tyrell Museum of Palaeontology, Drumheller, Canada.

### (a) *Anatomical observations of sutural mobility*

Four facial sutures commonly appear patent and slightly mobile in *T. rex* skulls observed. These are the maxilla–jugal, postorbital–jugal, quadratojugal–jugal and postorbital–squamosal contacts. Two of these sutures are not universally mobile: the quadratojugal–jugal suture is fused in some specimens (e.g. AMNH 5027) and movement at the postorbital–squamosal would be restricted by attachment of the superficial and possibly medial slips of the M. adductor mandibulae externus, which originate in part along the lateral supra-temporal fenestra margin. The remaining two sutures, namely the maxilla–jugal and postorbital–jugal contacts, remain patent in nearly all observed specimens, and are the main focus of this analysis. Patent, yet apparently immobile, sutures exist between many other cranial bones, and future analysis will attempt to elucidate the significance of these sutures. It should be noted that although the FEMs use a particularly loosely articulated skull (BHM 3033; figure 1) as a template, the following descriptions of cranial mobility are based on observations of numerous specimens (see above).

### (b) *Jugal–postorbital contact*

The postorbital laps a smooth groove running down half the length of the anterior surface of the ascending process of the jugal (figure 2*a*). Postorbital–jugal contact surfaces are variably rugose, with BHM 3033 bearing smooth articulation surfaces while ANMH 5027 and MOR 555 possess more rugose surfaces along the length of the contact. Furthermore, in AMNH 5027 and MOR 555, the anterior surface of the lower half of the ascending process bears a pronounced roughened region that marks the ventral extent of postorbital overlap. A depressed groove running along the posterior surface of the descending process of the postorbital marks the contact with the jugal. In all specimens observed and those documented in the literature (e.g. Brochu 2003) this contact is patent and potentially mobile, with the exception of MOR 008, in which the left jugal–postorbital contact is fused internally, probably as a result of the advanced age of this specimen (Molnar 1991). Additionally, minor interdigitations at the anterior edge of the postorbital–jugal suture in AMNH 5027 may have limited movement along the suture in this particular skull. Overlapping flanges at the postorbital–jugal contact surface generally prevent rotation in the transverse and parasagittal axis, but sliding of the jugal anteroventrally–posterodorsally against the postorbital is permitted (figure 2*a*).

### (c) *The maxilla–jugal contact*

The anterior portion of the jugal forks medially and laterally, ventral to its contact with the lacrimal. The medial fork laps on to the medial surface of the maxilla while the lateral fork further divides into a dorsal and ventral component, between which slots a narrow process of the maxilla (as noted by Molnar (1991)). Additionally the dorsal edge of an extended maxillary process laps the ventrolateral edge of the jugal along a posteriorly extended groove (figure 2*b*). In none of the observed specimens was the maxilla–jugal contact fused. Dorsoventral and mediolateral movement plus rotation about the transverse and parasagittal axes is prevented by the interlocking mediolateral and dorsoventral articulations. The distinct anteroposterior orientation of all contacts suggest that slight anteroposterior sliding movement plus some limited rotation about the longitudinal axis of the jugal is permitted at this suture (figure 2*b*).

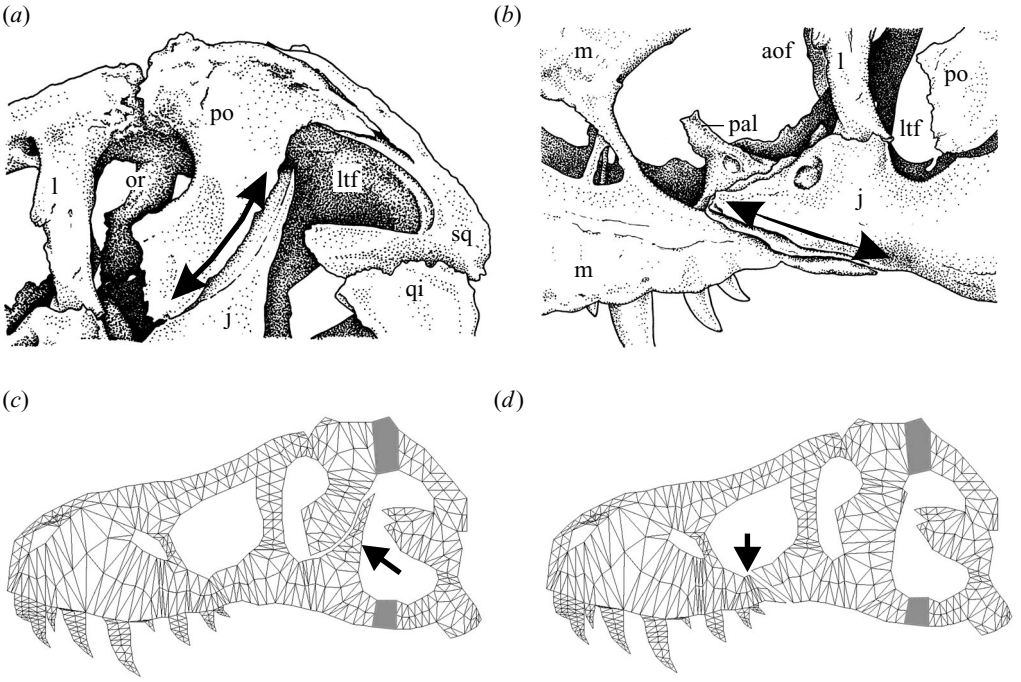


Figure 2. Sutural morphology and mobility. (*a*) Postorbital–jugal suture in *Tyrannosaurus rex*; (*b*) maxilla–jugal suture in *T. rex*; (*c*) 2D FEM of *T. rex* skull with mobile postorbital–jugal contact; and (*d*) 2D FEM of *T. rex* skull with mobile maxilla–jugal contact. Double-headed arrows indicate direction of slight adjustive movement at suture. Single-headed arrows indicate location of 'suture' in FE-mesh. Illustrations after BHM 3033. Grey areas and abbreviations as defined in figure 1; pal, palatine.

### (d) *Finite element modelling*

A two-dimensional (2D) FEM of a *T. rex* skull was created. A lateral-aspect photograph of BHM 3033 (Hell Creek Formation, South Dakota; figure 1*a*) was digitized in Scion Image (www.scioncorp.com). Outline *x*,*y* coordinates were imported into the Geostar geometry creator component of the Cosmosm FEA package (v. 2.0 for Unix; SRAC Corp. CA, USA and Cenit Ltd, UK). A series of 5 cm thick surfaces was created then 'meshed' to produce an interconnected grid of three-noded triangular FEs representing the lateral aspect of the cranium (figure 1*b*). Each element was attributed the mechanical properties of bovine Haversian bone after Rayfield *et al.* (2001).

The model represents a 2D section of the left aspect of the skull: the palate and braincase were not included. 2D models are used as a first approximation in orthopaedic biomechanical modelling, and using simple FEMs offers the potential to generate mechano-functional hypotheses (Carter *et al.* 1998), which may be further tested by digitally modifying future models. The 2D models presented here were constrained from moving about the lower temporal fenestra (figure 1*b*) to focus upon the stress response of the rostrum, which as a more planar structure than the posterior skull is more appropriate for 2D modelling. Stress patterns posterior to the constraining surfaces, including the effect of condylar and muscular forces in the posterior skull, were not analysed and this region of the skull should therefore be ignored in relevant figures.

Four structurally different FEMs were constructed by manipulating the base model: an initial 'fused' solid model with no mobile regions (figure 1*b*) and three modified 'mobile' models showing differing degrees of intracranial mobility; a mobile postorbital–jugal suture (figure 2*c*), a mobile maxilla–jugal suture (figure 2*d*), and a model with both a mobile maxilla–jugal and postorbital–jugal suture (not shown). The mobile FEMs (figure 2*c*,*d*) were created by introducing breaks in the FE-mesh at the location of the appropriate suture in the actual skull.

### (e) *Bite force magnitude and distribution*

*Tyrannosaurus rex* may have been capable of generating 13 400 N bite force at a single posterior tooth (Erickson *et al.* 1996). Using moment arm calculations to extrapolate this value rostrally along the tooth row, a total of 78 060 N was divided between biting teeth (therefore assuming 156 120 N bilaterally, less than, but approaching, values estimated by Meers (2002)). However, it may be argued that being first to contact a prey item, the large caniniform teeth received the majority of bite force (*sensu* Rayfield *et al.* 2001). In accordance with this suggestion, the two large caniniform teeth (figure 1*b*) were allocated 13 000 N each, while the smaller incisiform and posterior maxillary teeth were allocated lesser values scaled to the size of the teeth. In this model a total of 31 000 N was applied.

FEAs were performed to assess the stress response to this load in a fused or mobile skull. First, vertical dorsally directed bite forces representing the 'puncture' aspect of feeding were applied to the tooth tips in all four models and the corresponding stress and strain patterns were calculated. The analyses were then rerun applying instead a horizontally orientated, anteriorly directed bite force to represent the 'pull' tearing force, generated by the resistance of flesh and bone against the teeth during tugging and flesh-procuring behaviour (figure 1*b*). Multiple tearing analyses applying moment-calculated forces, variable tooth-size-related forces and equal forces to all teeth were investigated. Because bite force was hypothetical but identical in related models, relative rather than absolute patterns of stress and strain could be assessed.

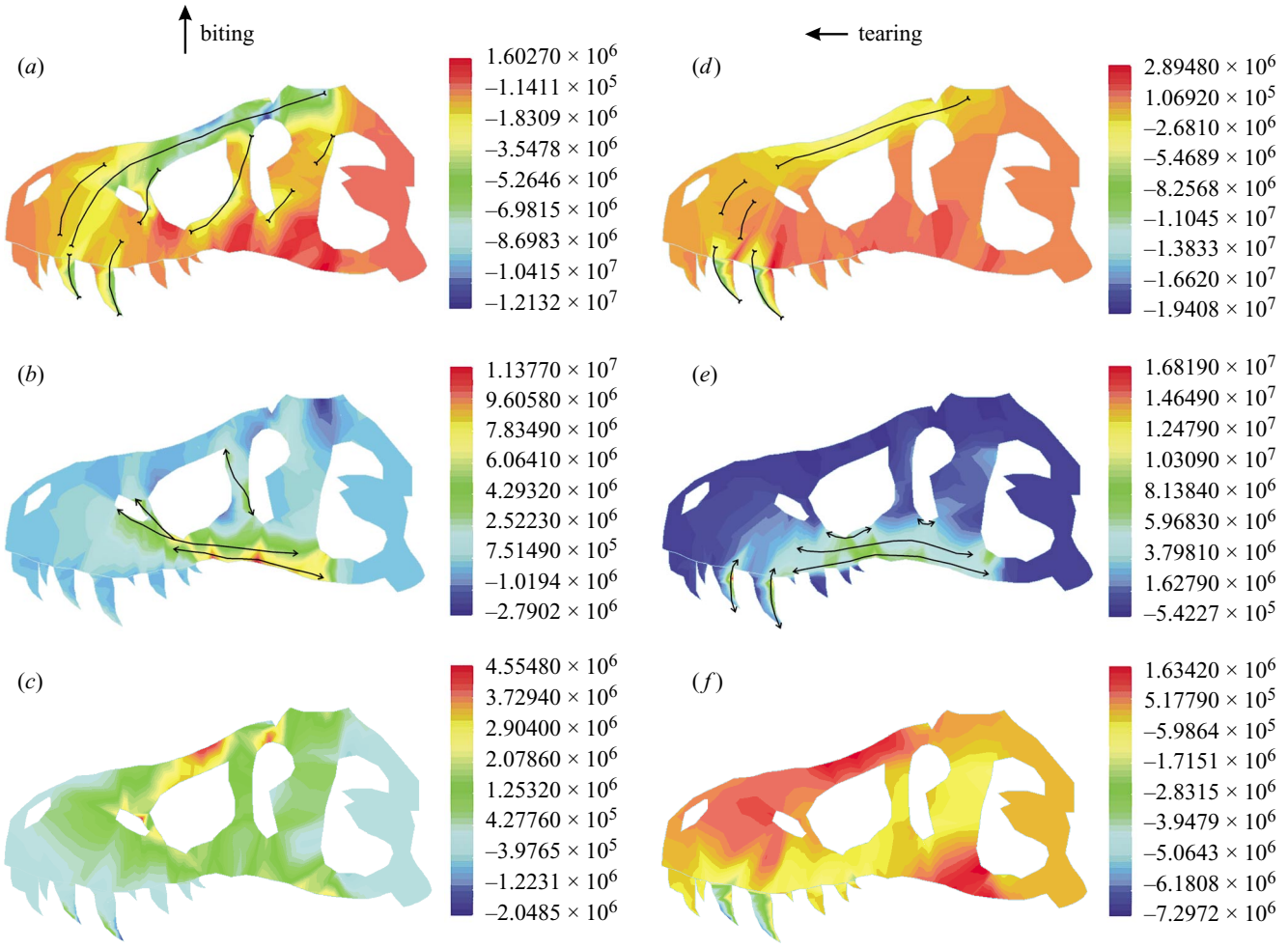


Figure 3. Stress in the fused FE *Tyrannosaurus rex* skull model generated by vertical biting (left column) or tearing (right column). (*a*) Principal stress 3 [P3], compressive stress; (*b*) P1 tensile stress; (*c*) shear stress; (*d*) P3 compressive stress; (*e*) P1 tensile stress; and (*f*) shear stress. Divergent arrows indicate orientation of tensile stress trajectories; convergent arrows indicate orientation of compressive stress trajectories. Units are Pa or $Nm^{-2}$. See electronic Appendix C for strain plots.

## 3. RESULTS

Colour-coded stress distribution plots with superimposed stress vector orientation illustrate the pattern of stress and strain in the skull under biting and tearing loads (figures 3 and 4 and electronic Appendices A–C). By convention, tensile stresses and strains are allocated positive values, whereas compressive stresses and strains are assigned negative values. Principal stresses (P1 tensile; P3 compressive), shear stress in the sagittal (here *XY*) 2D plane, normal *X*, normal *Y* and sagittal *XY* shear strain were recorded (the software does not calculate principal strains). Principal stresses record peak compressive and tensile stresses when shear stress equals zero. Peak tensile, compressive and shear stresses and strains were recorded and treated as an indicator of skull 'strength': higher peak stresses mean that less force is needed to induce yielding, therefore the skull is weaker. Regardless of bite force magnitude (moment-arm versus 'tooth-size' forces), nearly identical patterns of stress and strain were produced in models of the same geometry (although absolute magnitudes differ). It can be assumed that the stress patterns figured here apply to either biting regime.

### (a) *Stress in the fused-skull finite element model during biting and tearing*

Stress patterns in the vertical biting model (mimicking the 'puncture' phase of feeding) suggest that during biting, compressive stresses arc posterodorsally from the biting teeth through the maxilla and into the nasals and lacrimals (figure 3*a*). Stress vectors trace this curvature then become longitudinally orientated in the posterior region of the nasals and dorsal body of the postorbital (figure 3*a*). Peak tensile stresses are orientated longitudinally within the jugal and posterior maxilla, ventral to the lower temporal fenestra, orbit and antorbital fenestra (figure 3*b*). Tension follows the ventral rim of the antorbital fenestra, leaving the main body of the maxilla dorsal to the tooth row relatively untensed (figure 3*b*). Peak shear occurs in the nasals dorsal to the central antorbital fenestra and dorsal to the orbit (figure 3*c*).

When the biting simulation is altered to reflect pulling and tearing (hereafter known as the 'tearing' model), tensile vectors lose their anterodorsal component and trace the ventral edge of the skull (figure 3*e*). The largest maxillary teeth are subject to bending stress: the posterior tooth

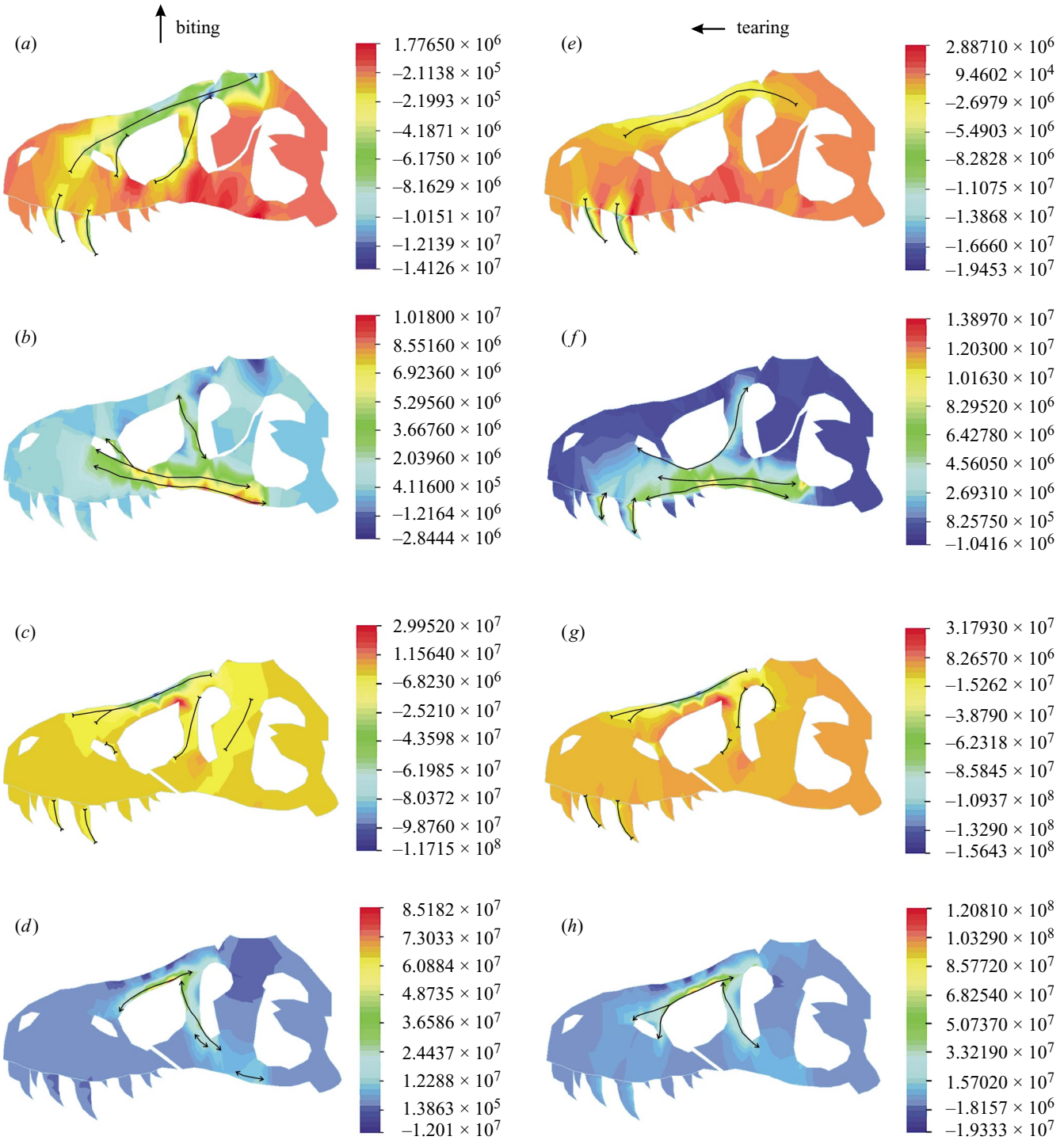


Figure 4. Stress in the mobile FE *Tyrannosaurus rex* skull models generated by vertical biting (left column) or tearing (right column). (*a*,*b*,*e*,*f*) have a mobile postorbital–jugal suture; (*c*,*d*,*g*,*h*) have a mobile maxilla–jugal suture. (*a*) Principal stress 3 [P3], compressive stress; (*b*) P1 tensile stress; (*c*) P3 compressive stress; (*d*) P1 tensile stress; (*e*) P3 compressive stress; (*f*) P1 tensile stress; (*g*) P3 compressive stress; and (*h*) P1 tensile stress. Divergent arrows indicate orientation of tensile stress trajectories; convergent arrows indicate orientation of compressive stress trajectories. Units are Pa or $Nm^{-2}$. See electronic Appendices B and C for shear stress and strain plots.

edge is tensed while the anterior edge compresses along its curvature (figure 3*d*,*e*). Compressive vectors are less obvious in the maxilla but longitudinally orientated compression is maintained in the dorsal maxilla, nasal and lacrimal (figure 3*d*). Large shear stresses are still observed in the nasals as during vertical biting, and the teeth are sheared also (figure 3*f*). Considering that the angle of bite force shifts by 90° from biting to tearing, stress distribution and orientation are surprisingly similar in both sets of models. There are, however, noticeable differences in stress–strain magnitude between the two loading conditions (table 1).

Table 1. Comparison of peak stress and strain values: owing to the simplistic nature of model, regard values as relative rather than absolute.
(Stress values are megapascals (MPa); strain values are microstrain ($\mu\varepsilon$); *X* or *Y* refers to direction of peak strain.)

| | | peak tensile stress (P1) | peak compressive stress (P3) | peak shear stress | peak tensile strain | peak compressive strain | peak *XY* shear strain |
|---|---|---|---|---|---|---|---|
| vertical biting | fused model | 11.4 | −12.1 | 4.6 | 1100 (*X*) | −1100 (*X*) | 1300 |
| | post.-jugal kinesis | 10.2 | −14.1 | 5.1 | 1160 (*X*) | −1300 (*X*) | 1620 |
| | max.-jugal kinesis | 85.2 | −117.0 | 43.2 | 12400 (*X*) | −11500 (*X*) | 12400 |
| | double kinesis | 85.2 | −117.0 | 43.2 | 12400 (*X*) | −11500 (*X*) | 12400 |
| tearing biting | fused model | 16.8 | −19.4 | 7.2 | 2080 (*Y*) | −1830 (*Y*) | 2170 |
| | post.-jugal kinesis | 13.9 | −19.5 | 7.3 | 2080 (*Y*) | −1820 (*Y*) | 2170 |
| | max.-jugal kinesis | 120.8 | −156.4 | 54.3 | 16190 (*X*) | −14320 (*X*) | 15810 |
| | double kinesis | 120.8 | −156.4 | 54.3 | 16200 (*X*) | −14330 (*X*) | 15810 |

### (b) *Predicting the effect of introducing cranial mobility from solid finite element models*

(i) *Maxilla–jugal suture*

This suture is located at the point of peak tensile stress in the biting skull model, and at a region of high magnitude (but not peak) tension in the tearing skull model (figure 3*b*,*e*). Tensile vectors are oriented along the predicted axis of suture movement (slightly more so in biting than tearing: compare figures 2*b* and 3*b*,*e*) and it is predicted that the introduction of suture mobility will act to reduce regional tensile stress, although whether the skull will be weaker or stronger is unclear. Small compressive vectors act perpendicularly to the axis of movement in the biting skull (not shown) and may operate to maintain contact of opposing joint surfaces.

(ii) *Postorbital–jugal suture*

Low-magnitude compressive vectors act along the long axis of the postorbital–jugal strut during biting and tearing, and tensile stresses are absent (figure 3*a–d*). This pattern is not congruent with the predicted axis of postorbital–jugal suture movement (figure 2*a*). It would therefore be predicted that mobilizing the postorbital–jugal suture should have a negligible effect upon stress distribution and overall strength of the skull under both biting regimes.

### (c) *The effect of introducing sutures into a finite element model*

As predicted, introducing a mobile postorbital–jugal suture into a FE-skull model has no notable effect on stress distribution and magnitude during biting and tearing (table 1 and compare figure 4*a*,*b* with figure 3*a*,*b* and figure 4*e*,*f* with figure 3*d*,*e*). Apart from a loss of compression in the postorbital bar (compare figure 3*a*,*d* with figure 4*a*,*e*) and marginal alterations to shear stress (see electronic Appendices A and B) in the mobile postorbital–jugal model, the stress environment and peak stresses and strain are practically identical to that of the fused skull.

Introducing a mobile contact at the maxilla–jugal suture removes tensile and shear stresses along the ventral region of the skull model. Peak tensile, compressive and shear stresses are instead concentrated in the posterior portion of the nasals and in the lacrimal dorsal to the antorbital fenestra (compare figure 3*a*,*b* with figure 4*c*,*d* and figure 3*d*,*e* with figure 4*g*,*h*; see electronic Appendices A and B for shear plots). Stress distribution is comparable during biting and tearing (compare biting figure 4*c*,*d* to tearing figure 4*g*,*h*). Dorsal to the antorbital fenestra, the skull experiences bending stresses as the lacrimal and possibly the posterior maxilla experience tension as the nasals are compressed (figure 4*c*,*d*,*g*,*h*). Although opening the maxilla–jugal suture has removed large tensile stresses from the ventral skull, peak stresses have been concentrated dorsal to the antorbital fenestra at magnitudes of 7 to 11 times greater than fused model peak stress–strain values (table 1). The dominant effect of the maxilla–jugal suture is such that the introduction of a second mobile joint at the postorbital–jugal contact has no modifying effect on mechanical performance and cranial stress patterns (see electronic Appendix A).

## 4. DISCUSSION

Stress–strain distribution and orientation are remarkably similar during simulations of both biting and tearing. Morphological features that resist biting loads are used equally in the resistance of tearing forces, meaning that the skull appears to be equally well adapted for the 'puncture' and 'pull' components of the proposed feeding strategy. Fused-skull models and those with a mobile postorbital–jugal suture are characterized by ventral tension and posterodorsally arcing compression from the tooth row to the skull roof, whereas models with a mobile maxilla–jugal suture experience bending stress in the roof of the snout, dorsal to the antorbital fenestra. Tensile and compressive patterns appear similar, but not identical, to those observed in a three-dimensional (3D) *Allosaurus fragilis* FEM during bilateral bite loading (Rayfield *et al.* 2001; figure 3).

### (a) *Rostral stress transmission*

It has been suggested that *T. rex* cranial suture morphology dictates that biting-induced compressive stresses pass directly from the maxilla to the nasals and bypass the maxilla–lacrimal contact (Hurum & Sabath 2003). FEMs confirm that compressive stresses do bypass the lacrimal when the maxilla–jugal suture is mobile (figure 4*c*,*g*). The maxilla–lacrimal contact is subject to large tensile bending stresses instead (figure 4*d*,*h*). The complex interlacing

morphology of the maxilla–nasal suture is consistent with the efficient accommodation of compressive strain and shock-absorption (Jaslow 1990) and the groove-like morphology of the maxilla–lacrimal contact suggests an adaptation to accommodate tensile strain across this suture. Nevertheless, when the maxilla–jugal suture is immobilized in the fused skull models, high-magnitude compressive stresses do pass directly from maxilla to lacrimal (figure 3*a*,*d* and 4*a*,*e*). This observation questions the distinctions drawn between the skulls of *T. rex* and *Tarbosaurus baatar* based upon compressive stress transmission (Hurum & Sabath 2003).

### (b) *Nasal robustness and rugosities*

Tyrannosaurid nasals are extremely rugose dorsally, and fused along the majority of their length, while the postorbitals display a dorsal, laterally expanded, thickened boss with a roughened surface (figures 1*a* and 2*a* 'po'). In all FEMs, peak compressive and shear stresses are concentrated in the nasals and dorsal portion of the postorbital, particularly when the maxilla–jugal suture is mobilized. The morphology of these rugose cranial bones suggests that they are optimized to withstand the type of compressive, shearing and bending stresses predicted by the FEM. As fused nasals are found in all tyrannosaurids and the tyrannosauroid *Eotyrannus lengi* (Hutt *et al.* 2001) perhaps we should expect to see similar patterns of cranial stress distribution in all members of the Tyrannosauroidea. In marked contrast, peak compressive and shear stresses accumulate in the fronto-parietal region rather than the nasals in biting *A. fragilis* FEMs (Rayfield 2001; Rayfield *et al.* 2001). As predicted by the FE-stress patterns, the frontals and parietals are fused or strongly sutured and thickened, and although the lateral borders of *A. fragilis* nasals are rugose, medially they are smooth elements meeting at a midline butt-joint that is often patent.

Nasal robustness and dorsal protuberances become more pronounced throughout *T. rex* ontogeny (Carr 1999) and this may be consistent with resisting greater bite forces in more mature individuals, if bite force scales with positive allometry to body mass and length as seen in the American alligator *Alligator mississippiensis* (Erickson *et al.* 2003). In an unusual example of less robust nasals (FMNH PR2081), prominent nasal protuberances are still observed dorsal to the antorbital fenestra (Brochu 2003), in the region predicted by the FEMs.

### (c) *Cantilever bending and lacrimal morphology*

Patterns of dorsal compression and ventral tension are consistent with the nasal region of the skull bending as a cantilever beam during biting. Even so, the presence of stress in the lacrimal and postorbital bars demonstrates that the skull does not act as a simple beam in the manner suggested by Molnar (2000), because the postulated neutral axis of bending in the region occupied by the interfenestral bars does in fact experience stress. Furthermore, modelled stress patterns in the lacrimal can be correlated with bony morphology as the axis of biting-induced compressive stress lies along a thin but medially prominent ridge of bone in the *T. rex* lacrimal (e.g. figures 3*a* and 4*a*). When the postorbital–jugal suture is open during tearing, this ridge withstands tensile stress instead (figure 4*f*).

### (d) *Tensile resistance*

According to FEMs, the postorbital–jugal suture did not play an active role in cranial stress accommodation, despite the sliding nature of the joint. The suture may not be mechano-functionally adapted or the position of model constraints may be affecting this result, and it should be investigated in future models. By contrast, FEMs suggest that the maxilla–jugal suture of *T. rex* was adapted to resist biting- and tearing-induced tensile strain in the ventral skull. Regardless of how mobile the sutures were in life, even minor adjustments in articulation would have served to protect bony tissue from damaging strains. The simple morphology of the maxilla–jugal suture is consistent with the observation that decreasing interdigitation and lack of fusion are associated with the presence of tensile strains at mammalian sutures (Rafferty & Herring 1999).

As a consequence of removing tension in the ventral skull, stresses and strains are directed elsewhere. In the case of the mobile maxilla–jugal model, stresses an order of magnitude greater than those generated in the fused model are experienced in the nasals, maxilla and lacrimal. During actual dynamic loading *in vivo*, sutural ligaments could act as shock-absorbers, absorbing tensile strain energy and reducing the magnitude of stress and strain in the dorsal skull, so increasing the adaptive significance of the suture. But it still appears fair to say that, as safety factors appear constant across taxa of all sizes, although higher in crocodilians than mammals and birds (Biewener 1982; Thomason & Russell 1986; Blob & Biewener 1999), the introduction of a mobile maxilla–jugal suture effectively 'weakens' the skull model, such that lower maximum bite forces can be tolerated, to maintain a constant ratio between stress generated during everyday use and peak yield stress (i.e. the safety factor). Although the maxilla–jugal suture is locally adapted to stress resistance, there is an overall functional cost of introducing this suture in terms of reduced skull strength. Fused skull models and those with mobility at the postorbital–jugal suture are 'stronger' and can tolerate higher maximum bite forces while maintaining a similar margin of safety.

The FEMs presented here are obviously crude representations of skull geometry and suture mobility. Strain-absorbing soft tissues are absent and loads are not transmitted across the suture as they are *in vivo* and *in vitro* (Buckland-Wright 1978; Thomason *et al.* 2001). Nevertheless, generating testable predictions and correlation of stress patterns to cranial morphology is possible using these simple models. Factors such as investigating the performance of a 3D model, altering the position of constraints and incorporating soft tissues at tooth sockets and further sutural contacts will all advance our understanding of *T. rex* cranial mechanical behaviour.

## 5. CONCLUSION

The cranium of *T. rex* appears equally well adapted to resist biting and tearing loading. This suggests that the puncture–pull feeding strategy inferred from tooth-marked bones is consistent with the mechanical construction and performance of the skull. Stress patterns predicted by FEMs are consistent with the bony morphology of the skull and a number of form–function adaptations can be identified.

(i) The robust nasals, positioned along the dorsal edge of the rostrum, act to resist compressive and shear stresses. This raises questions as to the evolution of tyrannosauroid nasal robusticity in relation to feeding behaviour: did the evolution of robusticity permit a shift in feeding strategy or did a novel strategy arise in which robusticity was advantageous?
(ii) The lacrimal is constructed to resist a complex suite of stresses found during simulated biting and tearing.
(iii) The maxilla–nasal contact acts to dissipate biting loads as previously suggested.
(iv) The maxilla–jugal suture appears to be adapted to resist tension in the ventral skull although at a cost of reduced cranial strength and capacity.

Sutural fusion appears to be controlled by an interplay of genetic and epigenetic factors (Herring 2000). The detrimental weakening effect of loosening the maxilla–jugal suture raises the possibility that mobility of sutures evolved in a correlated manner as an adaptive response to resist potentially damaging stresses generated during particular feeding styles, although the behaviour of the post-orbital–jugal suture challenges the idea that all sutures are functionally adaptive.

Using stress vectors generated in fused cranial models it is possible to predict the localized mechanical effect of introducing sutural mobility and the possible functional role and adaptive significance of the suture concerned. There is considerable potential for the use of FEA in the elucidation of patterns of cranial evolution, including the development of intracranial mobility within and across groups. However, steps towards modelling of soft tissues that are also integral to the behaviour of the cranium must be taken to achieve a more complete understanding of such morpho-functional evolutionary events.

This research was supported by the Natural Environment Research Council, UK, via postgraduate studentship (GT04/97/47/ES), an Emmanuel College Research Fellowship and a Royal Society equipment grant. For providing access to specimens in their care, I thank M. Norell (American Museum of Natural History), P. Larson (Black Hills Museum), J. R. Horner (Museum of the Rockies), P. R. Bjork (South Dakota School of Mines) and P. J. Currie (Royal Tyrell Museum of Palaeontology). D. B. Norman (Department of Earth Sciences, University of Cambridge) and P. Upchurch (Department of Earth Sciences, University College London) assisted in reading and commenting on earlier drafts of this manuscript.

## REFERENCES

Abler, W. L. 1992 The serrated teeth of tyrannosaurid dinosaurs, and biting structures in other animals. *Paleobiology* **18**, 161–183.

Abler, W. L. 1999 The teeth of the *Tyrannosaurus*. *Sci. Am.* **281**, 40–41.

Biewener, A. A. 1982 Bone strength in small mammals and bipedal birds: do safety factors change with body size? *J. Exp. Biol.* **98**, 289–301.

Blob, R. W. & Biewener, A. A. 1999 *In vivo* locomotor strain in the hindlimb bones of *Alligator mississippiensis* and *Iguana iguana*: implications for the evolution of limb bone safety factors and non-sprawling limb posture. *J. Exp. Biol.* **202**, 1023–1046.

Brochu, C. A. 2003 Osteology of *Tyrannosaurus rex*: insights from a nearly complete skeleton and high-resolution computed tomographic analysis of the skull. *J. Vert. Paleontol.* **22**(Suppl. 4), 1–138.

Buckland-Wright, J. C. 1978 Bone structure and the patterns of force transmission in the cat skull (*Felis catus*). *J. Morphol.* **155**, 35–62.

Buckley, L. 2003 Addressing the potential for cranial kinesis in *Tyrannosaurus rex*: a comparison of the palate complexes of *Tyrannosaurus rex* to *Varanus*. *J. Vert. Paleontol.* **23A**, 37A.

Carr, T. D. 1999 Craniofacial ontogeny in Tyrannosauridae (Dinosauria, Coelurosauria). *J. Vert. Paleontol.* **19**, 497–520.

Carter, D. R., Mikic, B. & Padian, K. 1998 Epigenetic mechanical factors in the evolution of long bone epiphyses. *Zool. J. Linn. Soc.* **123**, 163–178.

Chin, K., Toyaryk, T. T., Erickson, G. M. & Calk, L. C. 1998 A king-size theropod coprolite. *Nature* **393**, 680–682.

Erickson, G. M. & Olson, K. H. 1996 Bite marks attributable to *Tyrannosaurus rex*: a preliminary description and implications. *J. Vert. Paleontol.* **16**, 175–178.

Erickson, G. M., Van Kirk, S. D., Su, J., Levenston, M. E., Caler, W. E. & Carter, D. R. 1996 Bite-force estimation for *Tyrannosaurus rex* from tooth-marked bones. *Nature* **382**, 706–708.

Erickson, G. M., Lappin, A. K. & Vliet, K. A. 2003 The ontogeny of bite-force performance in American alligator (*Alligator mississippiensis*). *J. Zool. Lond.* **260**, 317–327.

Farlow, J. O., Brinkman, D. L., Abler, W. L. & Currie, P. J. 1991 Size, shape, and serration density of theropod dinosaur lateral teeth. *Mod. Geol.* **16**, 161–198.

Fastnacht, M., Hess, N., Frey, E. & Weiser, H.-P. 2002 Finite element analysis in vertebrate palaeontology. *Senck. Lethaea* **82**, 195–206.

Herring, S. W. 2000 Sutures and craniosynostosis: a comparative, functional, and evolutionary perspective. In *Craniosynostosis* (ed. M. M. Cohen & R. E. MacLean), pp. 3–10. Oxford University Press.

Herring, S. W. & Teng, S. 2000 Strain in the braincase and its sutures during function. *Am. J. Phys. Anthropol.* **112**, 575–593.

Hurum, J. H. & Sabath, K. 2003 Giant theropod dinosaurs from Asia and North America: skulls of *Tarbosaurus bataar* and *Tyrannosaurus rex* compared. *Acta Palaentologica. Polonica* **48**, 161–190.

Hutt, S., Naish, D. W., Martill, D. M., Barker, M. J. & Newbery, P. 2001 A preliminary account of a new tyrannosaurid theropod from the Wessex Formation (Early Cretaceous) of southern England. *Cret. Res.* **22**, 227–242.

Jaslow, C. R. 1990 Mechanical properties of cranial sutures. *J. Biomech.* **23**, 313–321.

Jaslow, C. R. & Biewener, A. A. 1995 Strain patterns in the horncores, cranial bones and sutures of goats (*Capra hircus*) during impact loading. *J. Zool. Lond.* **235**, 193–210.

Jenkins, I. 1997 Finite element analysis of skull dynamics in Permian synapsid (mammal-like-reptile) carnivores. *J. Morphol.* **232**, 271.

Jenkins, I., Thomason, J. J. & Norman, D. B. 2002 Primates and engineering principles: applications to craniodental mechanisms in ancient terrestrial predators. *Senck. Lethaea* **82**, 223–240.

Larson, P. L. 1998 Cranial morphology, mechanics, kinesis and variation in *Tyrannosaurus rex*. In *Dinofest International Symposium III, Program and Abstracts* (ed. D. L. Wolberg, K. G. S. Miller, L. Carey & A. Raynor). Philadelphia, PA: Academy of Natural Sciences.

Meers, M. B. 2002 Maximum bite force and prey size of *Tyrannosaurus rex* and their relationship to the inference of feeding behaviour. *Hist. Biol.* **16**, 1–12.

Molnar, R. E. 1991 The cranial morphology of *Tyrannosaurus rex*. *Palaeontol. Abt.* A **217**, 137–176.

Molnar, R. E. 2000 Mechanical factors in the design of the skull of *Tyrannosaurus rex* (Osborn 1905). *Gaia* **15**, 193–218.

Molnar, R. E. & Farlow, J. O. 1990 Carnosaur paleobiology. In *The Dinosauria* (ed. D. B. Weishampel, P. Dodson & H. Osmolska), pp. 210–224. Berkeley, CA: University of California Press.

Rafferty, K. L. & Herring, S. W. 1999 Craniofacial sutures: morphology, growth and *in vivo* masticatory strains. *J. Morphol.* **242**, 167–179.

Rafferty, K. L., Herring, S. W. & Marshall, C. D. 2003 Biomechanics of the rostrum and the role of facial sutures. *J. Morphol.* **257**, 33–44.

Rayfield, E. J. 1998 Finite element analysis of the snout of *Megalosaurus bucklandi*. *J. Vert. Paleontol.* **18**, 71A.

Rayfield, E. J. 2001 Cranial design and function in a large theropod dinosaur: a study using finite element analysis. PhD thesis, University of Cambridge, UK.

Rayfield, E. J., Norman, D. B., Horner, C. C., Horner, J. R., May Smith, P., Thomason, J. J. & Upchurch, P. 2001 Cranial design and function in a large theropod dinosaur. *Nature* **409**, 1033–1037.

Rayfield, E. J., Norman, D. B. & Upchurch, P. 2002 Prey attack by a large theropod dinosaur: reply. *Nature* **416**, 388.

Smith, K. K. & Hylander, W. L. 1985 Strain gauge measurement of mesokinetic movement in the lizard *Varanus exanthematicus*. *J. Exp. Biol.* **114**, 53–70.

Snively, E. & Russell, A. 2002 The Tyrannosaurid metatarsus: bone strain and inferred ligament function. *Senck. Lethaea* **82**, 35–42.

Thomason, J. J. 1995 To what extent can the mechanical environment of a bone be inferred from its architecture? In *Functional morphology in vertebrate paleontology* (ed. J. J. Thomason), pp. 249–263. Cambridge University Press.

Thomason, J. J. & Russell, A. P. 1986 Mechanical factors in the evolution of the mammalian secondary palate: a theoretical analysis. *J. Morphol.* **189**, 199–213.

Thomason, J. J., Grovum, L. E., Deswysen, A. G. & Bignell, W. W. 2001 *In vivo* surface strain and stereology of the frontal and maxillary bones of sheep: implications for the structural design of the mammalian skull. *Anat. Rec.* **264**, 325–338.

As this paper exceeds the maximum length normally permitted, the author has agreed to contribute to production costs.

Visit www.journals.royalsoc.ac.uk and navigate to this article through *Proceedings*: Biological Sciences to see the accompanying electronic appendices.